Geophysical and Astrophysical Convection, pp. 00-00
Gordon and Breach Science Publishers

TURBULENT CONVECTION: WHAT HAS ROTATION TAUGHT US?

JOSEPH WERNE[1,2]

[1] *National Center for Atmospheric Research*
P.O. Box 3000, Boulder, CO 80307-3000

[2] *Joint Institute for Laboratory Astrophysics &*
Laboratory for Atmospheric and Space Physics
University of Colorado, Boulder, CO 80309-0440

Rotation alters turbulent convection in fundamental ways. Thermal plumes forming on domain boundaries spin-up and rotate faster than the external rotation rate. Their shapes differ from plumes in nonrotating convection, as do their basic motions. They participate in vigorous lateral mixing with neighboring plumes as they mutually advect. Unstable mean density stratification results. Despite these changes, other aspects of nonrotating convection remain (*e.g.*, the nonclassical heat-transport efficiency $Nu \sim Ra^{2/7}$ is seen in both cases). The similarities shared by and differences between rotating and nonrotating convection teach us much about turbulent transport in general.

1 Introduction

There are examples in nature where turbulent fluid motion is induced by buoyancy, then molded by rotation. These include many astrophysical and geophysical flows, from solar and giant planetary convection to oceanic deep convection. In each case, differential heating initiates convective motion while spinning of the star or planet provides the basic rotation of the fluid. Ordered structures and flow coherence often result and can dominate the dynamics, features not anticipated by classical stochastic theories of turbulence. Plumes and vortices, overturning circulations, zonal jets, and ocean gyres are seen.

Attempts to characterize some of the fundamental aspects of buoyancy induced turbulence have proceeded through laboratory and numerical studies of incompressible convection. The highly nonlinear nature of the flows make purely theoretical inquiry extremely difficult (or impossible) without guidance from empirical sources. In this paper I highlight some of the important discoveries provided by recent laboratory experiments on turbulent Rayleigh-Bénard convection, both in rotating tanks and in stationary vessels, and the theoretical ideas they have inspired. I then describe new numerical solutions for rotating convection (computed by Keith Julien, Sonya Legg, James McWilliams and me) which help evaluate some of the theoretical assumptions.

2 Nonrotating Rayleigh-Bénard convection

Rayleigh-Bénard convection is a classic experiment in which a fluid layer is heated from below. The magnitude of the buoyancy force which results is measured by the non-dimensional Rayleigh number $Ra = g\alpha\Delta L^3/\nu\kappa$, where Δ is the temperature drop maintained across the layer's depth L. g is the local acceleration due to gravity. α, ν, and κ are the fluid's thermal expansion coefficient, kinematic viscosity, and thermal diffusivity, respectively. For values of Ra larger than $O(10^3)$, buoyancy overcomes diffusive processes, and convective motion ensues (Chandrasekhar, 1961). For much larger values of Ra, $O(10^7)$, only very sharp gradients in the flow fields may elevate viscous drag and thermal diffusion sufficiently to balance the excessive buoyancy force. As a result, at these large Rayleigh numbers thin shear layers and thin thermal plumes participate in the fluid dynamics (Heslot *et al.*, 1987; Castaing *et al.*, 1989; see also Chapter ??). The Rayleigh numbers appropriate to geophysical and astrophysical fluid layers, such as the earth's planetary boundary layer, the oceanic mixed layer, and the solar convection zone, are much larger, attaining values of the order 10^{18}. The flows that result at such high Rayleigh numbers possess 1) many thin plumes which punctuate the buoyancy and motion fields at small scales, but also 2) sufficient dynamic range for plumes to act collectively to organize larger scales of motion.

In 1989, Sano, Wu & Libchaber hinted at the ability of plumes to organize larger scales of convective motion in their low-temperature Helium-gas experiments (Sano *et al.*, 1989). A single persistent turbulent roll filled their 8.7 cm tall, 8.7 cm diameter vessel for $Ra > 4\times 10^7$. Though such a unit aspect (width-to-height) ratio roll does not evoke an image of 'large scale', for Ra below 4×10^7 (but $> 3 \times 10^5$), single rolls are unstable, frequently reversing orientation.[1] More dramatic evidence for large-scale coherence in laboratory convection is offered by Krishnamurti's $40\times 40\times 1$ experiments with water (Krishnamurti, 1995). Even in this very wide container, a domain-filling pattern develops in which plumes cluster together and march in 'soldier-row' formation across the cell.

The organized motions in these experiments affect the transport properties of the fluid layer. For example, at Rayleigh numbers above which plumes spontaneously appear, the heat-transport law for flux through the layer becomes less efficient. Heslot *et al.* report $Nu \sim Ra^{1/3}$ when no plumes are present, but $Nu \sim Ra^{2/7}$ for $Ra > 4 \times 10^7$ (Heslot *et al.*, 1987). They christened the 2/7 state 'hard turbulence' and dubbed the 1/3 regime 'soft'. Similarly, Krishnamurti sees inefficient heat transport in her organized plumey flows, actually consistent with an even smaller exponent: 1/4 (Krishnamurti, 1995). Here the Nusselt number $Nu = H/(\kappa\Delta/L)$ is the normalized heat flux H. Though the small difference between these exponents can appear academic when the data are plotted on a logarithmic axis (which is typical), when a linear axis is used the difference is clearly sizeable. For example, at $Ra = 10^{18}$ the 1/3 law predicts more than three times the heat transport than does the 2/7 law (for laws that coincide at $Ra = 4 \times 10^7$).

The experiments by Libchaber and coworkers have drawn a good deal of attention from theorists for one important reason: their impressive range in Ra. By using Helium gas near its triple point ($\sim$ 5 K), Ra up to 10^{15} has been obtained (Wu & Libchaber, 1992). Over seven decades in Ra means the exponent can be determined to at least three significant digits. Also, just three decades shy of geophysical and astrophysical values, the experiments promise relevance to realms of turbulence occurring in nature. With these motivations, theorists have attempted explanation of the 2/7 exponent.

[1] Despite the axisymmetric geometry of the container, the rolls in these experiments flowed only in a single plane, pinned by the few thermal probes used to record fluid temperatures (Sano *et al.*, 1989).

3 Turbulent convection theories

3.1 Priestley's theory

Before reviewing modern theories for turbulent convection, it is instructive to review the classic theory for the 1/3 law; it is due to Priestley (Priestley, 1954, 1959; see also Howard, 1966; Malkus, 1963; Spiegel, 1962). Priestley suggested that all of the temperature drop imposed across a fluid layer should concentrate in thin thermal layers adjacent to the top and bottom boundaries. The reason for this partitioning of the flow is that while turbulent motion efficiently transports heat in the interior of the layer, only diffusive processes act at the domain boundaries where the normal velocity is zero. The heat flux H through the entire layer can therefore be estimated by measuring the thickness λ of these thermal boundary layers: $H \approx \Delta/2\lambda$, from which we have $Nu \approx L/2\lambda$. Priestley further argued that for sufficiently large values of L (or equivalently Ra), the thin boundary layers should be incapable of communicating to each other across the turbulent layer separating them; hence, $\lambda \neq \lambda(L)$. With these two expressions and the definition for Ra, it is readily shown that $Nu \sim Ra^{1/3}$.

3.2 Kadanoff, Zaleski & Zanetti's theory

Because thermal plumes appeared simultaneously with the 2/7 law in the experiments of Heslot *et al.*, the first theoretical attempt by Kadanoff, Zaleski & Zanetti to derive the 2/7 law concentrated on plumes (Castaing *et al.*, 1989). They conjectured a 'mixing zone' where plumes grow out of the boundary layers, then mix through turbulent agitation before merging with the bulk fluid. The crux of their argument is that the dynamics of plumes are dominated by two competing effects: buoyancy and drag. Their picture of plumes consists of fragmented pieces of highly unstable boundary layers with temperatures $\Delta/2$ and thicknesses λ. As these plumes move under the buoyancy force $g\alpha\Delta/2$, viscous drag $\nu u/\lambda^2$ acts to slow them. Here u is the plume velocity. Balancing these two, we obtain an expression relating u and λ:

$$\frac{uL}{\kappa} \sim Ra\left(\frac{\lambda}{L}\right)^2 . \tag{1}$$

In addition to Eq. (1), Kadanoff, Zaleski & Zanetti made use of earlier attributions to turbulent convection, namely Priestley's relation for λ and Nu

$$Nu \sim \frac{L}{\lambda} , \tag{2}$$

and Prandtl's view of the turbulent bulk (Prandtl, 1932) in which the heat flux is carried by eddy motion, $H \sim u_c\Delta_c$, or

$$Nu \sim \left(\frac{u_c L}{\kappa}\right)\left(\frac{\Delta_c}{\Delta}\right) , \tag{3}$$

and the kinetic energy of the eddies is gained at the expense of buoyancy work as they traverse the layer, $u_c^2 \sim g\alpha\Delta_c L$, or

$$\left(\frac{u_c L}{\kappa}\right)^2 \sim \sigma Ra\frac{\Delta_c}{\Delta} . \tag{4}$$

Here Δ_c and u_c are measures of the temperature and velocity of the dominant eddies in the turbulent interior. The system is closed with the argument that as plumes merge with the bulk turbulence, they attain velocities consistent with the interior: $u \sim u_c$. Combining the four expressions Eqs. (1)–(4) for the four unknowns Nu, u_c, Δ_c, and λ, the 2/7 law is derived (along with other laws for u_c and Δ_c). All of the resulting laws agree with experimental observation (Castaing *et al.*, 1989 for Nu and Δ_c; Shen *et al.*, 1995 for u_c).

3.3 Shraiman & Siggia's theory

In 1990, Shraiman & Siggia proposed an alternate theory (Shriaman & Siggia, 1990). This time plumes would not be the central players, but rather only the intermediaries necessary to organize the large-scale circulation. In fact, Shraiman & Siggia propose the 2/7 law emerges precisely when the dominant circulation is fast enough to produce shear-flow turbulence near the boundaries. They estimate the dissipation in the layer as $\varepsilon \approx u_*^3/L$, where $u_* = \sqrt{\nu(\partial U/\partial z)_{wall}}$ is the friction velocity, U being the mean velocity parallel to the boundary (wall) and z the normal direction (*e.g.*, Tennekes & Lumley, 1972). For such wall-bounded turbulent-shear layers, very near the wall (in the so-called viscous sub-layer) the velocity profile is linear $U = z(\partial U/\partial z)_{wall}$ (*e.g.*, Tennekes & Lumley, 1972). By assuming a thermal boundary layer λ so thin that it nestles within the viscous sub-layer, Shraiman & Siggia simplify the heat equation and obtain the result

$$Nu \sim (\partial U/\partial z)_{wall}^{1/3} \ . \tag{5}$$

Then, employing the exact relation (Shraiman & Siggia, 1990)

$$\frac{\varepsilon L^4}{\kappa^3} = \sigma Ra(Nu - 1) \ , \tag{6}$$

the asymptotic ($Nu \gg 1$) scaling laws $Nu \sim Ra^{2/7}$ and $(\partial U/\partial z)_{wall} \sim Ra^{6/7}$ are obtained. The new prediction for the wall stress has been directly verified with 2D numerical simulation (Werne, 1993).

3.4 Cautionary comment on scaling theories

The stark contrast between these two approaches points to the caution with which one must digest scaling theories for turbulent fluids: derivation of a known result does not guarantee the underlying assumptions sufficient to realize the behavior in nature. For theoretical approaches to laboratory convection to be useful to those who model natural flows at $Ra \sim O(10^{18})$, the necessary and key dynamical ingredients responsible for the observed transport laws must be identified. Is the mere presence of plumes enough to restrict the heat flux, as Kadanoff, Zaleski & Zanetti suggest? Or do boundary conditions play a crucial role as suggested by Shraiman & Siggia? Or is another theoretical description in fact correct?

3.5 She's theory

She offered an alternate view to Kadanoff, Zaleski & Zanetti in the same year, 1989 (She, 1989). He suggests a simple modification to Kolmogorov's 1941 description of homogeneous and isotropic turbulence (Kolmogorov, 1941), one that includes buoyancy. Two major changes accompany the inclusion of buoyancy: 1) anisotropic forcing and 2) non-conservative cascades of energy to dissipative scales. She's theory incorporates only the latter. He proposes Kolmogorov's well-known scaling law relating the velocity of an eddy v_ℓ to its size

ℓ, $v_\ell \sim \varepsilon^{1/3}\ell^{1/3}$, be modified to include injection of energy from the buoyancy force: He suggests

$$v_\ell \sim \varepsilon^{1/3}\ell^{1/3}\left(\frac{\ell}{\delta}\right)^\beta \quad . \tag{7}$$

Here δ is the thermal dissipation scale of the flow, and β is a constant exponent. Like Kadanoff, Zaleski & Zanetti, She also employs Prandtl's arguments for turbulent convection,

$$H_\ell \sim v_\ell \Delta_\ell \qquad \text{and} \qquad v_\ell^2 \sim g\alpha\Delta_c \ell \ , \tag{8}$$

only here She considers quantities appropriate to the scale ℓ of individual eddies. A noteworthy exception to this rule, however, is the suggestion that eddies of all scales gain kinetic energy at the expense of buoyancy work from the *largest scale*, possessing the temperature Δ_c. By examining Eqs. (7) and (8) at both scale L and δ, and by suggesting the equivalence of δ and λ, She obtains $\beta = 1/6$ as well as the 2/7 law. She's computed spectrum for turbulent convection derived in this theory has not been seen in experiment or simulation.

3.6 Yakhot's theory

The fourth and final attempt to derive the 2/7 law is due to Yakhot (Yakhot, 1992). Like She, Yakhot concentrates on spectral properties and modifies one of Kolmogorov's turbulence formulas to include buoyancy effects. The starting point here is Kolmogorov's so-called 4/5 law for velocity differences in decaying homogeneous and isotropic turbulence (Kolmogorov, 1941). Yakhot suggests that on sufficiently small scales, the turbulent pressure field reorients and isotropizes motions initiated by buoyancy, eventually leading to isotropic fields on these small scales. He suggests, therefore, that Kolmogorov's 4/5 relation applies to small scales, with only the minor addition of a randomly oriented buoyancy-work term. Yakhot then proceeds to suggest a scaling theory by examining velocity differences at large separations of order L. A few errors are made by Yakhot, such as proposing an eddy diffusivity inconsistent with the exact result $Nu = N$ where N is the total thermal dissipation in the layer. Nevertheless, these technical errors can be corrected (Werne, 1996) and, with She's assumption ($\delta \approx \lambda$), the 2/7 law can in fact be derived.[2] Despite this achievement, a major conceptual flaw in the theory is the employment of isotropic gravity to deduce scaling behavior. It is certain that on the largest scales of motion, gravity is anisotropic; since these scales dominate the transport characteristics, randomly oriented gravity is a questionable concept on which to base a global transport theory.

4 Rotating Rayleigh-Bénard convection

When a convecting fluid layer is rotated, basic changes in the dynamics take place. Both the detailed motions of plumes and their collective interaction are affected. One might expect, therefore, that the global transport properties (*e.g.*, the total heat flux) should also exhibit dependence on rotation.

In 1969, Rossby was the first to conduct an extensive study on rotating Rayleigh-Bénard convection (Rossby, 1969). With two parameters to vary, Ra and Ta, instead of only one, data collection can be overwhelming. Nevertheless, Rossby presents an impressive series of Nu

[2] Without correcting the error $Nu \neq N$, She's assumption leads to $Nu \sim Ra^{5/19}$ in Yakhot's paper. Only when one takes $Nu \sim N$ does the 2/7 exponent result.

curves in Ra - Ta space. The non-dimensional Taylor number $Ta = (2\Omega L^2/\nu)^2$ is proportional to the square of the rotation rate Ω. His data span $0 < Ta < 10^8$ and $0 < Ra < 10^7$, with individual experiments sufficiently numerous to individually plot smooth contours of $Nu \in [1, 1.5, 2, 2.5, 3, 4, 5, 6, 7, 8, 9, 10, 11, 12]$. Though quantitative conclusions are difficult to draw from Rossby's data, most importantly because the aspect ratio is varied between some experimental series,[3] it appears that Nu is relatively less sensitive to Ta (than to Ra) for sufficiently large Ra.

More recently, Zhong *et al.* report new experiments in rotating Rayleigh-Bénard convection (Zhong *et al.*, 1993). Like Rossby, Zhong *et al.* use a cylindrical vessel; theirs has aspect ratio 2. Visualizations of their flow at $Ra = 7 \times 10^6$ and $Ta = 1.8 \times 10^7$ reveal motions of interacting vortices which swirl cyclonically (in the direction of rotation $\vec{\Omega}$) before spiraling toward each other and finally merging. Spinning plumes have been seen in convection experiments before (Nakagawa & Frenzen, 1955; Rossby, 1969; Boubnov & Golitsyn, 1986); however, Zhong *et al.* were the first to quantify the co-rotation rate and merger dynamics.

In addition to these studies on Rayleigh-Bénard convection between rigid, constant-temperature boundaries, other experiments target configurations more appropriate to geophysical flows. For example, Boubnov & Golitsyn (1986, 1990) study steady-state convection bounded by a rigid, constant-heat-flux surface below and a free surface above; Fernando *et al.* (1991) use a similar configuration to study the transient dynamics when bottom heating is turned on instantaneously; finally, Maxworthy & Narimousa (1994) initiate a surface buoyancy flux through salt release, either through the entire upper surface or confined to a smaller patch. Though the results from these studies are interesting, particularly as they address the role rotation plays in determining characteristic length- and velocity scales, here we concentrate only on statistically steady Rayleigh-Bénard convection to focus our discussion. For speculation on the role rotation plays in deep oceanic convection, see Chapter ??.

5 Numerical simulation of rotating convection

To illustrate some of the aspects of rotating convection discovered experimentally (and mentioned above), as well as some new results, I now present numerical solutions computed by Julien, Legg, McWilliams & Werne. The algorithm used is a pseudo-spectral Fourier/Chebyshev-'tau' method developed by Keith Julien and me. Side boundaries are periodic, while the top and bottom surfaces are held at fixed temperatures. Separate series of calculations are performed with no-slip and stress-free velocity conditions. All simulations resolve the dissipation scale. For more details on the simulations, see Julien *et al.*, 1996b.

5.1 Intermittent flow fields

Figure 1 presents the temperature and vertical vorticity on slices through the three-dimensional domain at increasing values of Ra and Ta. For all simulations, the ratio Ra/Ta is held fixed at $(0.75)^2$ so as to keep rotation and buoyancy time-scales comparable. The Prandtl number $\sigma = \nu/\kappa$ is 1.0. The associated color tables for the figure are included in Figure 1b. From the figure we see that the horizontal scale of convection decreases as Ta is increased; this is predicted by linear stability calculations. The horizontal line at the bottom of each column in the figure indicates the wavelength of the most unstable linear mode. At low Ra,

[3]Rossby's experiments include aspect ratios ranging from 6.4 to 31. He does not report the value of the aspect ratio for individual data points on his $Nu(Ra, Ta)$ diagram.

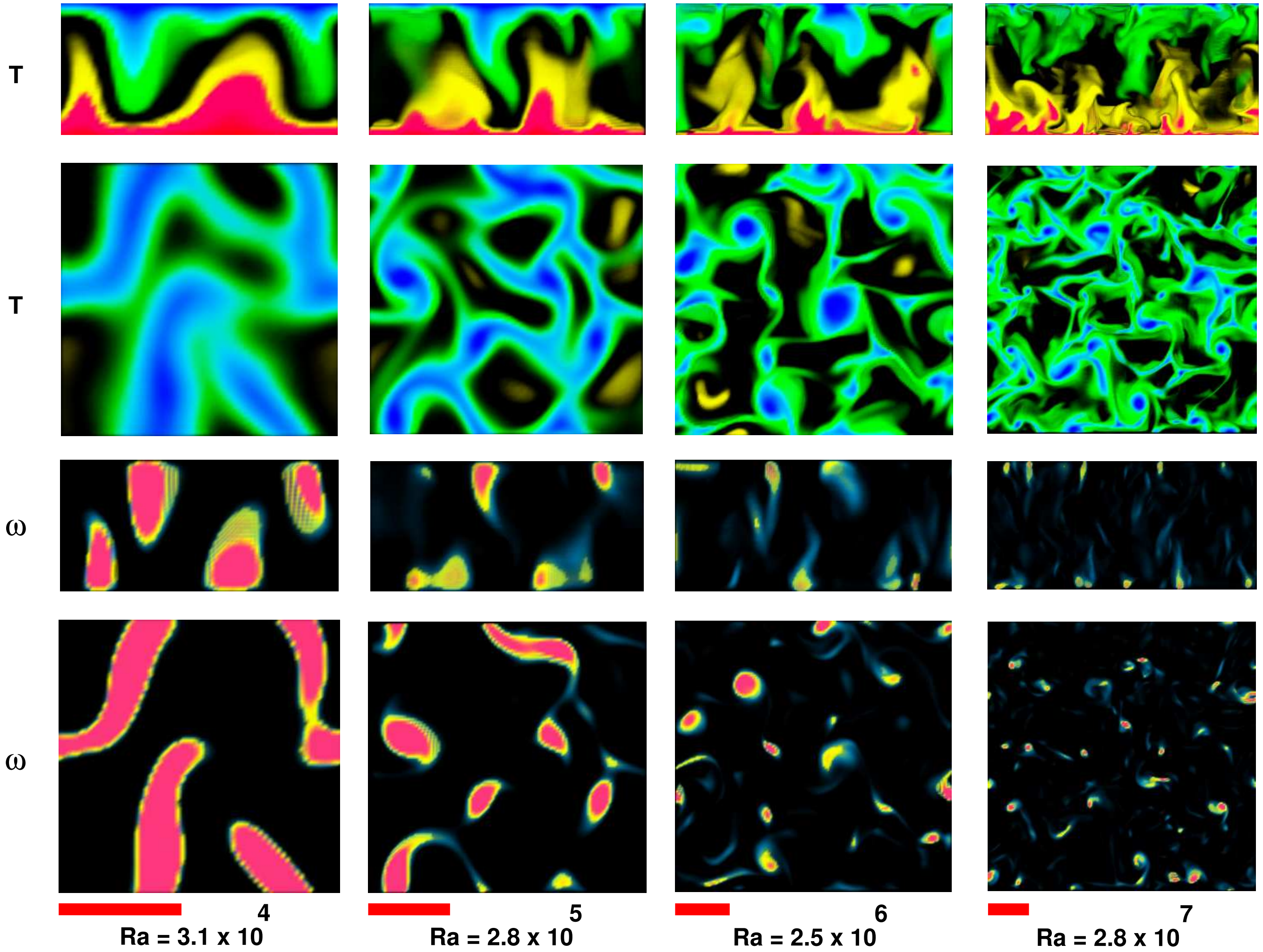

Figure 1a: Temperature and vertical vorticity for rapidly rotating convection. Views from side and above.

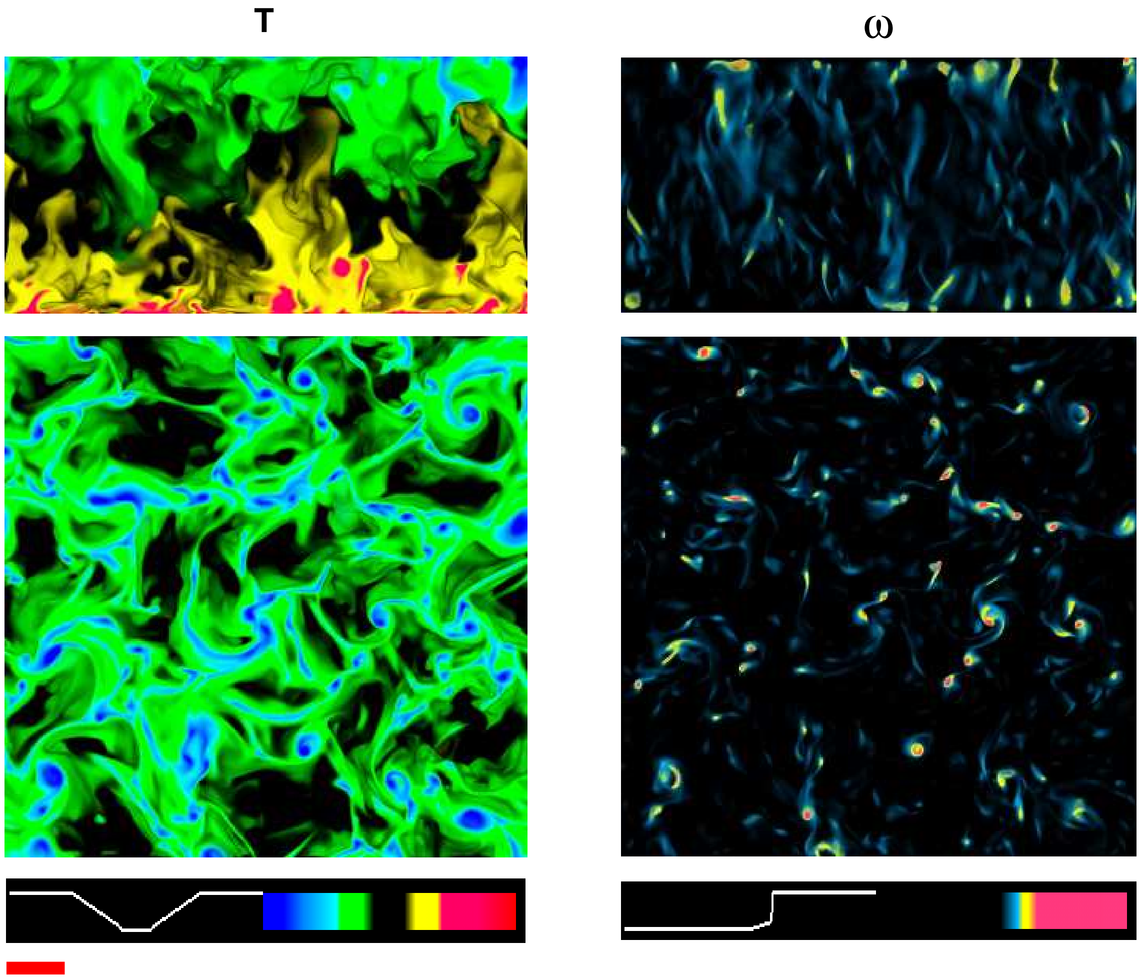

Figure 1b: Temperature and vertical vorticity for Ra=1.1 x 10^8 and Ta=2 x 10^8.

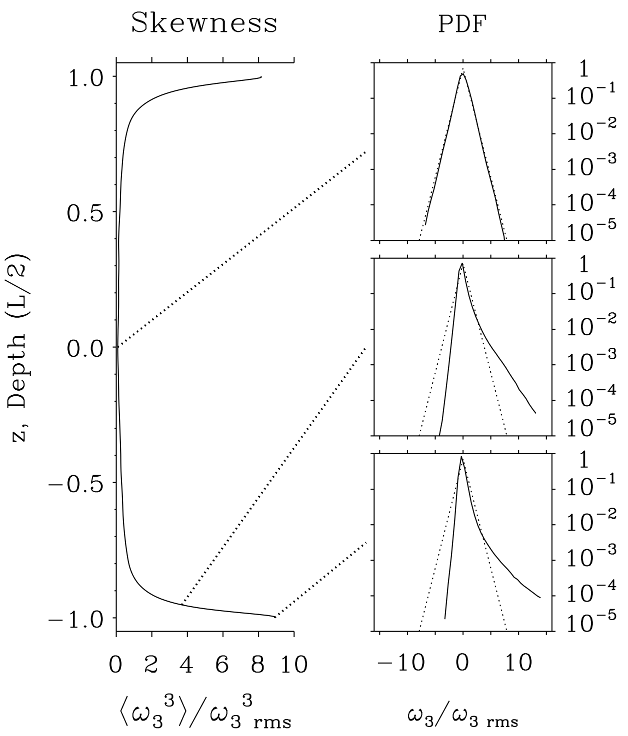

Figure 2: Vertical-vorticity skewness and PDFs for rotating Rayleigh-Bénard convection between no-slip boundaries. Exponential (dotted) PDFs are also included for references.

convection takes on the pattern of chaotic rolls (Figure 1a, $Ra = 3.1 \times 10^4$). For increasing Ra, however, the fields become punctuated by more closely spaced plumes; see Figure 1a, $Ra \geq 2.5 \times 10^6$. By $Ra = 1.1 \times 10^8$, the temperature field is filled with sharp thermal structures; see Figure 1b.

5.2 Cyclonic plumes

The vorticity is even more intermittent than the temperature. This is evident in both Figure 1 and the probability density functions (PDFs) for the two fields (Julien *et al.*, 1996a). Strong correlation exists between cyclonic vorticity and thermal plumes, as was observed in the experiments (Nakagawa & Frenzen, 1955; Rossby, 1969; Boubnov & Golitsyn, 1986; Zhong *et al.*, 1993). The cyclonic relative spinning of plumes results from angular momentum constraints: as plumes grow from perturbations on the boundary-layer, they form tubes which extend vertically away from the boundary; their angular velocity amplifies as they contract in the horizontal direction, much like an ice skater pulling in her arms.

Figure 2 illustrates the cyclonic skewing of plume vorticity through the profile of vertical-vorticity skewness, $\langle \omega_3^3 \rangle / \omega_3^3{}_{rms}$. Here, averages over horizontal planes and time are indicated by $\langle\ \rangle$. PDFs at three points within the layer are also plotted. Near the boundary where plumes form, the skewness is high, and the associated PDF reflects large numbers of intense

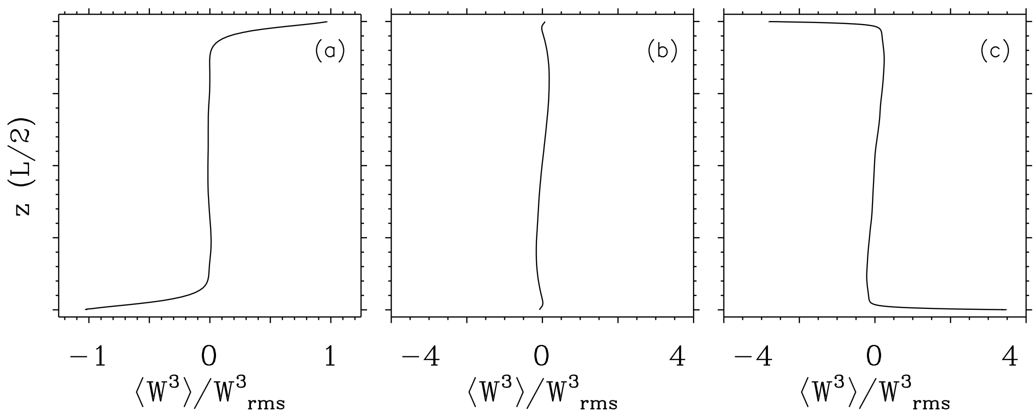

Figure 3: Vertical-velocity-skewness profiles. (a) $Ra = 10^7$, $Ta = 0$, no-slip boundaries. (b) $Ra = 1.8 \times 10^8$, $Ta = 3.2 \times 10^8$, stress-free. (c) $Ra = 1.1 \times 10^8$, $Ta = 2 \times 10^8$, no-slip.

cyclonic events. As plumes are pulled into the interior by buoyancy, their cyclonicity is dramatically reduced. Values close to zero occur at mid-layer where turbulent interactions between plumes mix and reorient them.

5.3 Ekman pumping

A consequence of intense cyclonic rotation for plumes can include Ekman pumping (Ekman, 1905; Gill, 1982), depending on the boundary conditions. Consider a vortex tube that terminates at a plane boundary. If the tube is in geostrophic balance (with outward centrifugal acceleration $(2\vec{\Omega}+\vec{\omega}) \times \vec{v}$ balanced by an inward radial pressure-gradient force $\vec{\nabla}P$), then the nature of the velocity conditions determines the circulation pattern around the tube. For no-slip boundaries, the centrifugal acceleration drops to zero at the surface (because $\vec{v} = 0$). Hence, the pressure gradient prevails there, resulting in a radial in-flow of fluid. In order to conserve mass flow, the radial in-flow must be compensated by an expulsion away from the boundary along the tube axis in z. Stress-free conditions do not produce this kind of shear-induce Ekman pumping because the velocity need not be zero at the boundary.

To illustrate the role Ekman pumping plays in rotating convection, Figure 3 shows the vertical-velocity skewness $\langle W^3 \rangle / W^3_{rms}$ versus depth z for three different simulations. Profile (a) contains the skewness for nonrotating convection between no-slip boundaries. As was found by Moeng & Rotunno, near the boundaries, motion is skewed toward incoming fluid, the dominant dynamics being that of plume bombardment from the opposite boundary (Moeng & Rotunno, 1990). Profile (c) shows results for rotating convection. Here Ekman effects are clearly evident. Strong pumping away from the boundaries is indicated by the outward skewing of the velocity field. This is exactly opposite to the nonrotating result (a). Profile (b) presents results for rotating convection between stress-free boundaries. Here Ekman pumping is absent, as expected. Furthermore, the bombardment from incoming plumes is also absent, which might not have been expected. As we shall see, rotation dramatically increases the mixing dynamics between plumes, making traversal of the entire layer (and bombardment of the opposite boundary) unlikely.

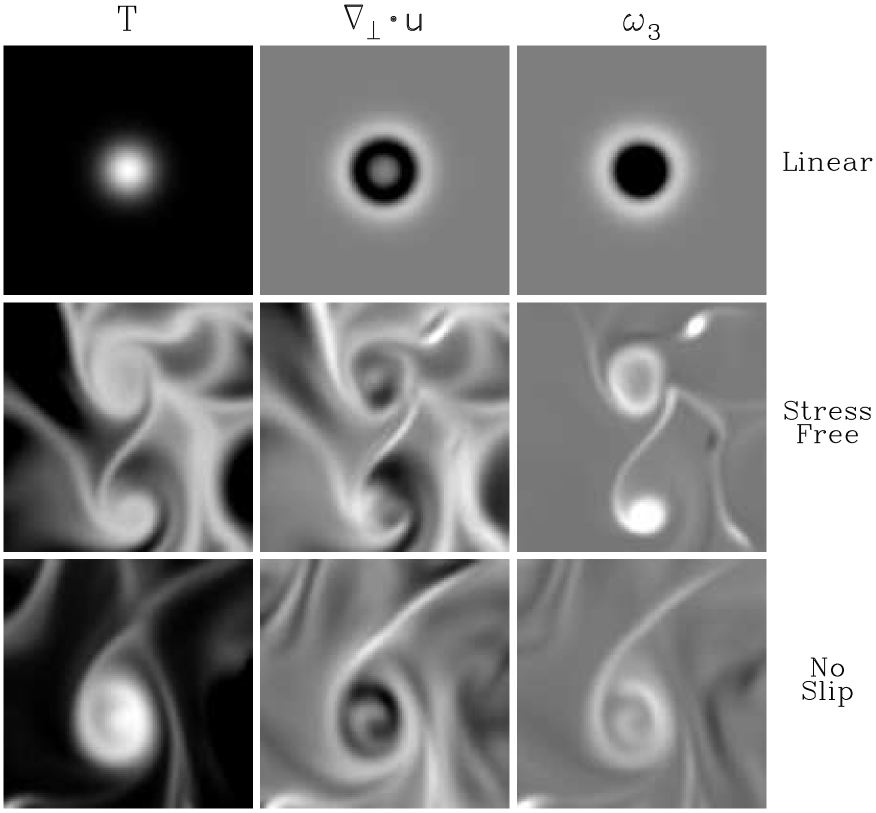

Figure 4: Temperature, horizontal divergence, and vertical vorticity on a horizontal plane through developing plumes. The top row depicts fields for the thermal Ekman layer resulting from a Gaussian-shaped 'plume' on the thermal boundary layer; see text. The middle (bottom) row displays fields for numerical simulations with stress-free (no-slip) boundaries within (slightly above) the mean hot thermal boundary layer. The shading is lighter for more intense temperatures, horizontal convergence, and cyclonic flow.

5.4 Linear thermal Ekman layer

A feature of plumes in rotating convection is their distinctive shape when compared to nonrotating convection. Figure 4 shows some typical features exhibited by plumes when viewed from above. In particular, in rotating flows, plumes tend to have ring-shaped cross-sections, especially for the divergence and vertical vorticity fields. These features are present in both stress-free and no-slip simulations. A simple linear model of plume formation in the boundary layers predicts this ring shape.

Consider a linear thermal Ekman layer whose pressure and horizontal velocity fields are described by the boundary-layer approximation:

$$fv \approx \nu \partial_{zz} u - \partial_x P \ , \tag{9}$$

$$-fu \approx \nu \partial_{zz} v - \partial_y P \ , \tag{10}$$

$$\partial_z P \approx g\alpha T \ . \tag{11}$$

T is a prescribed temperature field, normally taken in the classic Ekman-layer analysis to be zero (Ekman, 1905; Gill, 1982). Here let us consider the simple boundary-layer model

$$T = \begin{cases} 1 - z/\lambda & z < \lambda \\ 0 & z > \lambda \end{cases} \tag{12}$$

with $\lambda(x, y)$ a function of the horizontal directions x and y. u and v are the horizontal velocity components, P is the pressure divided by density, and f is the Coriolis parameter 2Ω. Because the system (9)–(11) is linear, solutions are straightforward to compute; one must take care to match the velocity fields and their derivatives at $z = \lambda$. Solutions are of the form $X = X_E + X_{th}$ where X is the horizontal velocity field in complex notation $X = u + \mathrm{i}v$. X_E is the classic Ekman-spiral solution obtained for $T = 0$; *i.e.*, $X_E = q^{-1}\partial_z X_0(1 - \mathrm{e}^{-qz})$ for no-slip boundaries, and $X_E = constant$ for stress-free. Here q is the inverse Ekman layer thickness $q = \sqrt{\mathrm{i}f/\nu}$, and $\partial_z X_0$ denotes the wall stress at $z = 0$. X_{th} has a more complicated form $X_{th} = (\Lambda/q^4\lambda^2)\, R(q\lambda, qz)$ where $\Lambda = \partial_x\lambda + \mathrm{i}\partial_y\lambda$ depends on horizontal gradients in λ, and R is a function of $q\lambda$ and qz.[4] Note that for λ independent of x and y, $X_{th} = 0$. For a Gaussian-shaped bump, $\lambda = \mathrm{e}^{-(x^2+y^2)/2}$, X_{th} results in the horizontal divergence and vertical vorticity shown in the top row of Figure 4. Interestingly, local Ekman pumping can in fact act near a stress-free boundary, as is evident in the computed horizontal divergence field (see also Hide, 1964). Nevertheless, the positive pumping in the ring circling the Gaussian bump is compensated (exactly) by the negative pumping within the ring; therefore, no net thermal Ekman pumping results. Though details in the computed fields differ from this simple analysis (presumably because of an imperfect prescription for T), general features are shared by both.

5.5 Nonlinear Ekman spirals

Though the linear analysis just presented correctly predicts the qualitative shapes of plumes as they emerge from the boundary layers, its quantitative value is limited because of the high degree of nonlinearity in the plumes. To demonstrate, Figure 5a compares the predicted linear Ekman spiral (dotted curve) with three hodographs — plots of $v(x_i, y_i, z)$ versus $u(x_i, y_i, z)$ — at slightly different horizontal positions near a plume. Nonlinear effects are evident in the numerical solutions by their more tightly spiraling velocity fields (Carrier, 1971; McWilliams, 1971). The locations (x_i, y_i) at which the hodographs are produced are indicated in Figure 5c on a plane positioned just above the mean thermal boundary layer. These locations are chosen to include the 'core' of a plume, the 'ring' region at the edge of a plume, and the region just 'outside' a plume for $Ra = 1.1 \times 10^8$. The solid dot on the classic solution marks the height to which the simulation results are plotted, roughly twice the thermal boundary-layer thickness. Hodographs are normalized by $q/\partial_z X_0$ and rotated by 45° so they may be compared easily.

While the core and outside regions exhibit substantial variability from plume to plume (due to different plume 'ages' and different instantaneous flow conditions external to the plume), the ring region appears better defined with similar Ekman spirals for different plumes. In fact, for sufficiently high Ra ($Ra \geq 2.5 \times 10^6$), the tightness of the Ekman spiral (*i.e.*, the nonlinearity) in the ring region appears to saturate, producing spirals of nearly identical shape for plumes at different Ra; see Figures 5b and 5d. Solutions with $Ra < 2.5 \times 10^6$ exhibit weaker Ekman spirals, tending toward the classic linear solution as Ra (and hence, the nonlinearity) is decreased.

[4] For the exact form of $R(q\lambda, qz)$, see Julien *et al.*, 1996b.

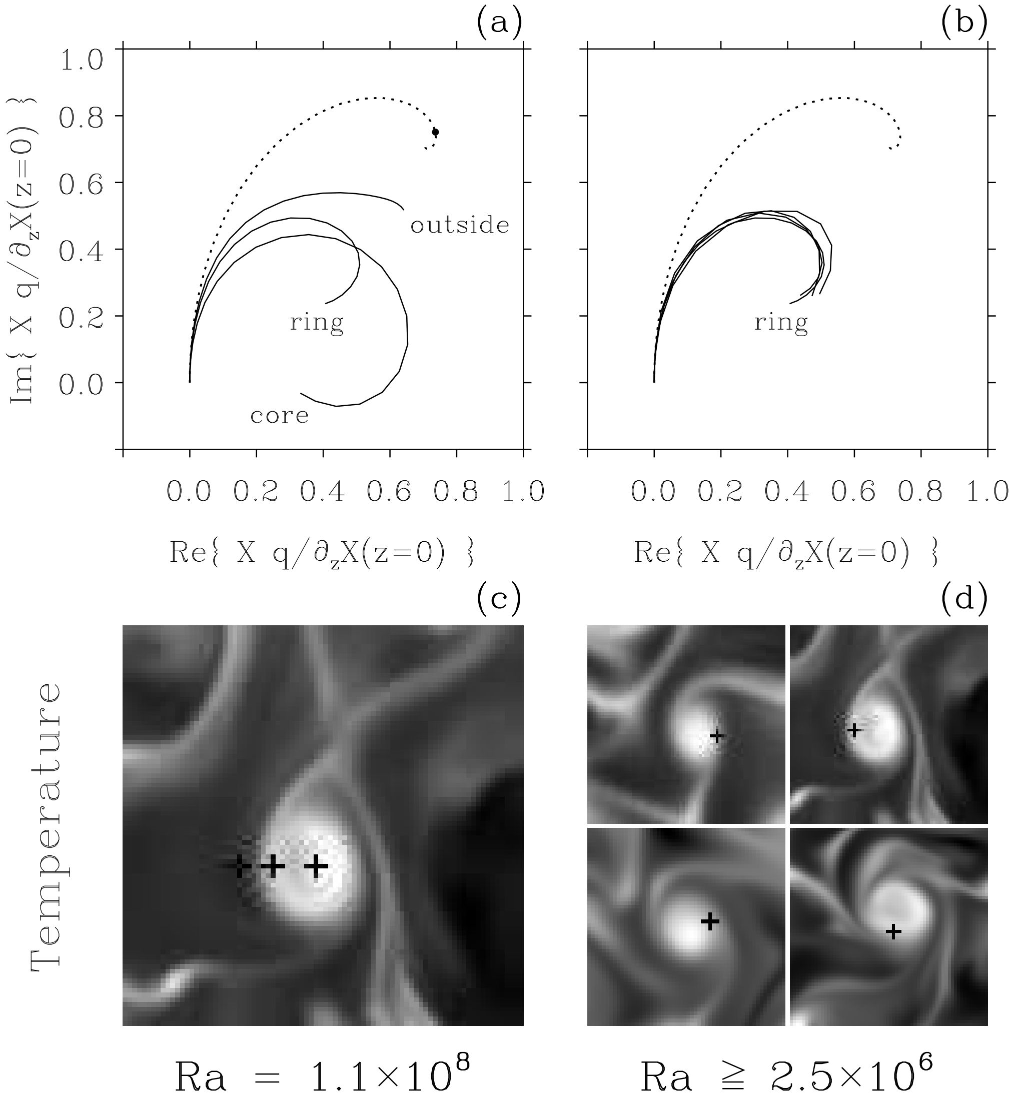

Figure 5: (a,b) Velocity hodographs ($v(x_i, y_i, z)$ versus $u(x_i, y_i, z)$ at a single horizontal location (x_i, y_i)) associated with plumes over no-slip boundaries. (a) Hodographs within the 'core' of a plume, in the 'ring' region at the edge of a plume, and just 'outside' a plume for $Ra = 1.1 \times 10^8$. (b) Hodographs in the ring region of plumes for high Ra ($Ra = 2.5 \times 10^6$, 8.4×10^6, 2.8×10^7 and 1.1×10^8). (c) Temperature on a plane just above the hot thermal boundary layer for $Ra = 1.1 \times 10^8$. Hotter fluid is depicted with lighter shades. Crosses indicate the locations of the hodographs in (a). (d) Temperature above the boundary layer for the four values of Ra depicted in (b). Ra increases from left to right with the highest Ra shown in the upper right corner and the lowest in the lower left.

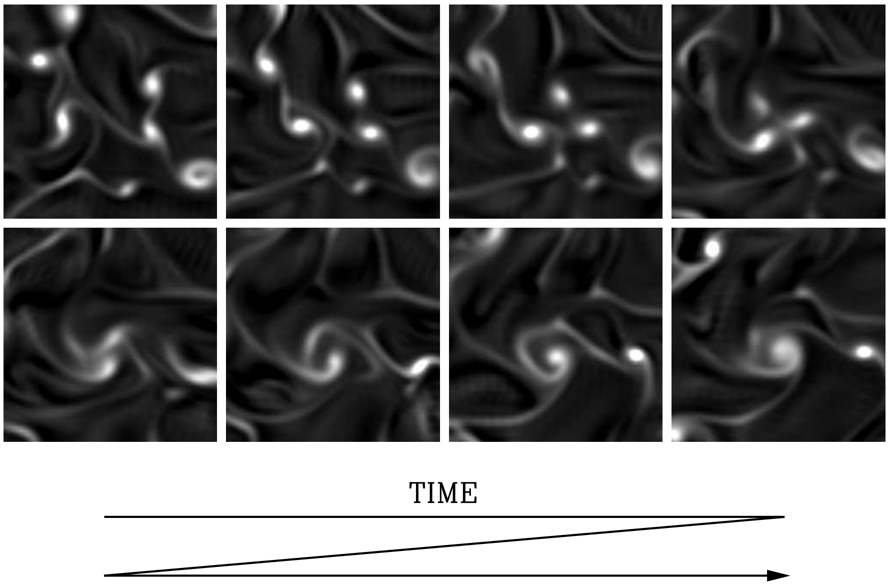

Figure 6: Merger of three vortex filaments over a no-slip boundary. $Ra = 8.4 \times 10^6$. Temperature on a plane just above the hot boundary layer is shown with lighter shades depicting hotter fluid. Since plumes intensify cyclonic vorticity, the light spots also indicate centers of strong vorticity.

5.6 Plume-plume interactions

Having discussed the manner in which the dynamics of isolated plumes are changed by external rotation, it is useful now to characterize how rotation molds the interactions between plumes. As is stated above, all of the plumes in our simulations rotate cyclonically. Therefore, mutual advection of neighboring plumes induces co-rotation. When sufficiently close, co-rotating plumes eventually merge, as Zhong *et al.* observe. Furthermore, if the dynamical time-scale for advection is short compared to diffusive processes, mergers must be accompanied by filamentation and expulsion of some of the vorticity from the plumes (Melander *et al.*, 1988). Figure 6 illustrates the merger and associated filamentation of three neighboring plumes in simulations with no-slip boundaries.

The mutual advection, filamentation, and merger dynamics of a multi-vortex system provides an efficient means to stir the flow field laterally, mixing fluid properties in horizontal planes. Because plumes and vortices are more numerous and more closely packed at higher Ta, vortical interactions and, hence, lateral mixing will be enhanced. The end result is dilution of plume temperature (and an accompanying enhancement of the background temperature) as plumes are mixed with ambient fluid. As a result, only very few plumes survive the tortuous journey across the layer, explaining the absence of boundary bombardments when rotation is sizeable (Figure 3b). Furthermore, at each incremental level away from the boundaries, fewer plumes survive, the spent plumes having deposited all of their thermal content into the background nearer the boundary from which they originated. We should expect, therefore, a reduction in the background intensity of temperature as we move

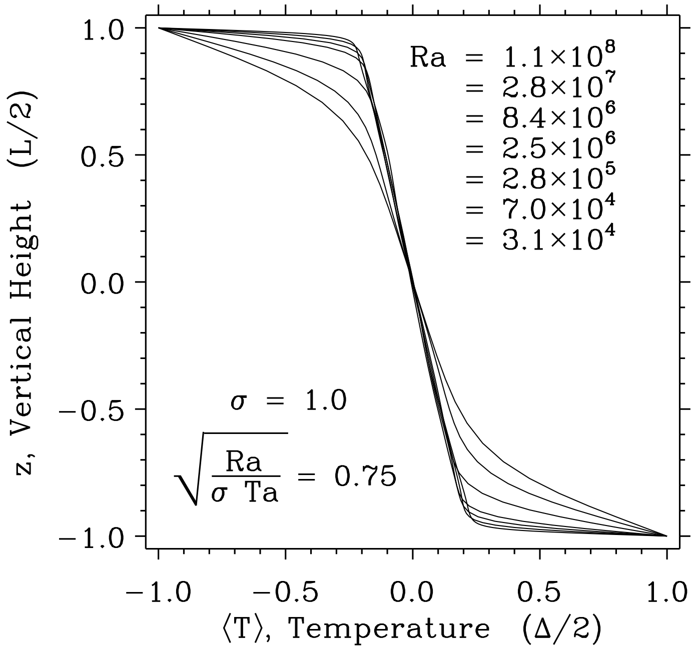

Figure 7: Profiles of mean temperature with height z. All solutions shown possess no-slip boundaries.

away from the boundaries, and hence, a mean unstable stratification when lateral mixing is intense.

Figure 7 shows profiles for temperature with depth at increasing Ra and Ta (holding Ra/Ta fixed). Higher Ra curves possess sharper boundary layers at $z = \pm 1$. The expected mean stratification in the interior is observed and persists (and in fact saturates) at high Ra. Mean thermal gradients have also been observed in laboratory rotating convection (Fernando *et al.*, 1991; Boubnov & Golitsyn, 1990; Hart & Ohlsen, 1996; Ecke, 1996). In contrast, in nonrotating Rayleigh-Bénard convection, temperature is adiabatically stratified with a negligible mean gradient observed outside the thermal boundary layers (*e.g.*, Belmonte *et al.*, 1993).

5.7 Rotating hard turbulence

Despite the many changes rotation brings to turbulent convection, the heat-transport law is virtually unchanged. Figure 8 shows the computed convective heat transfer, $Nu-1$, versus Ra for both no-slip and stress-free solutions. Remarkably, the no-slip solutions exhibit exactly the same scaling behavior (2/7 law) as nonrotating convection experiments. The scaling behavior of the rms vertical velocity and temperature at mid-layer, *i.e.*, u_c and Δ_c, is also identical to the nonrotating case (Julien *et al.*, 1996b).[5]

[5]After we reported the 2/7 law for rotating convection at fixed Ra/Ta (Julien *et al.*, 1996a,b), Ecke *et al.* were the first to observe the result in laboratory experiments (Ecke, 1996). Hart & Ohlsen also study rotating

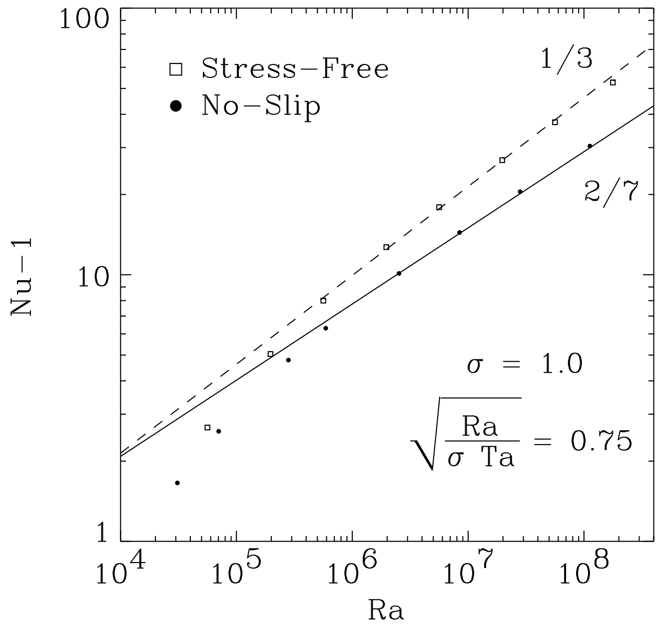

Figure 8: Convective heat transport $(Nu-1)$ versus Ra for both no-slip and stress-free boundaries. The uncertainty in Nu results from the finite numerical integration times used and is less than or equal to the size of the plotting symbols.

Stress-free results are also included in the figure. These numerical solutions do not have analogous laboratory counterparts because the slippery surfaces simulated are unphysical. Interestingly however, at the onset of scaling behavior, Priestley's 1/3 law emerges. By $Ra = 4 \times 10^7$ the heat transport becomes slightly less efficient, apparently when the Ekman and thermal boundary layers cross (Julien *et al.*, 1996b). Of course with such a limited range of possible scaling with Ra (10^6–10^8), it is difficult to distinguish two power laws from a different functional form; however, it is clear that the initial behavior of Nu for $Ra > 10^6$ differs between the no-slip and stress-free cases. For more details on the rotating hard-turbulent state, see Julien *et al.*, 1996a,b and Hart & Ohlsen, 1996.

6 Conclusions

In brief summary, the many changes rotation brings to turbulent convection include vortical plumes of ringed shape, Ekman pumping, reduced horizontal length scales, vortex-vortex interactions, mutual advection, enhanced lateral mixing, and mean thermal gradients in the bulk. Despite these myriad changes, rotating solutions with no-slip boundaries exhibit the same 2/7 law for heat transport observed for nonrotating laboratory convection. This is a remarkable result. With plume dynamics dramatically different for rotating and nonrotating

hard turbulence, but they do not directly measure Nu (Hart & Ohlsen, 1996).

flows, identical scaling suggests the relative unimportance of the detailed dynamics of plumes to a general theory for transport in turbulent convection. This is all the more confounding in light of the fact that the appearance of plumes heralds a change in the global transport (*e.g.*, the emergence of the 2/7 law) in nonrotating laboratory experiments.

Sense can be made of these facts when we consider that stress-free solutions exhibit a different heat-transport law. Apparently, boundary details are crucial. Though coherent structures in the form of plumes are required to organize motions necessary for the 2/7 law, reduced heat transport does not occur unless the organized shearing motions act on no-slip boundaries. Of the four turbulent transport theories currently competing to derive the 2/7 law, only Shraiman & Siggia's predicts different behavior for stress-free and no-slip boundaries.

In the opening remarks of NCAR's 1995 summer meeting inspiring these collected works, Kerry Emanuel mentioned laboratory convection and the 2/7 exponent. He speculated that differences in laboratory and real-world boundary conditions could prove crucial in determining the applicability (or inapplicability) of the 2/7 law to atmospheric convection. As we see from the work reported here, Emanuel's assessment is accurate. Even so, the correct transport laws for turbulent atmospheric, oceanic, and solar convection remain unknown. To advance we must evaluate the nature of coherent motions on small scales in natural flows and address how the dynamics couple with real-world boundaries to set flux-transport laws. Work addressing topography relevant to the Earth's planetary boundary layer has already begun with convection experiments over 'rough' surfaces (Shen *et al.*, 1996). Nevertheless, much fundamental fluid-dynamic research remains to be done. In future work addressing geophysical and astrophysical fluids (for which boundaries are neither perfectly flat nor no-slip), we may find utility in individual aspects of several of the turbulent-transport theories discussed here.

Acknowledgements

I have learned much about rotating convection from my enthusiastic experimental friends Dan Ohlsen and Bob Ecke, and my collaborators Keith Julien, Sonya Legg and James McWilliams. This work was partially supported by NCAR's Advanced Study Program, NCAR's Visiting Scientist Program, and NSF HPCC grant ECS9217394. Computations were carried out at the Pittsburgh Supercomputing Center under grant MCA935010P. NCAR is sponsored by the National Science Foundation.

References

Belmonte, A., Tilgner, A. & Libchaber, A. "Boundary layer length scales in thermal turbulence." Phys. Rev. Lett. 70, 4067–4070 (1993).

Boubnov, B. M. & Golitsyn, G. S. "Experimental study of convective structures in rotating fluids." J. Fluid Mech 167, 503–531 (1986).

Boubnov, B. M. & Golitsyn, G. S. "Temperature and velocity field regimes of convective motions in a rotating plane fluid layer." J. Fluid Mech. 219, 215–239 (1990).

Carrier, G. F. "Swirling flow boundary layers." J. Fluid Mech. 49, 133–144 (1971).

Castaing, B., Gunaratne, G., Heslot, F., Kadanoff, L., Libchaber, A., Thomae, S., Wu, X.-Z., Zaleski, S. & Zanetti, G. "Scaling of hard thermal turbulence in Rayleigh-Bénard convection." J. Fluid Mech. 204, 1–39 (1989).

Chandrasekhar, S. "Hydrodynamic and Hydromagnetic Stability." Oxford University Press (1961).

Ecke, R. private communication (1996).

Ekman, V. W. "On the influence of the earth's rotation on ocean-currents." Arkiv. Matem. Astr. Fysik, Stockholm, 2–11, 1–52 (1905).

Fernando, H. J. S., Chen, R-R. & Boyer, D. L. "Effects of rotation on convective turbulence." J. Fluid Mech. 228, 513–547 (1991).

Gill, A. E. "Atmosphere-Ocean Dynamics," Academic Press, New York (1982).

Hart, J. E. & Ohlsen, D. R. "Laboratory experiments on rotating turbulent convection." preprint (1996).

Heslot, F., Castaing, B. & Libchaber, A. "Transitions to turbulence in helium gas." Phys. Rev. A 36, 5870–5873 (1987).

Hide, R. "The viscous boundary layer at the free surface of a rotating baroclinic fluid." Tellus 16, 523–529 (1964).

Howard, L. N. "Convection at high Rayleigh number." In Proc. of the 11th Int. Congr. of Appl. Mech. Munich (Germany) (ed. H. Gortler). pp. 1109-1115. Springer, Berlin (1966).

Julien, K., Legg, S., McWilliams, J. & Werne, J. "Hard turbulence in rotating Rayleigh-Bénard convection." Phys. Rev. E 53, 5557R–5560R (1996a).

Julien, K., Legg, S., McWilliams, J. & Werne, J. "Rapidly rotating turbulent Rayleigh-Bénard convection." J. Fluid Mech. 322, 243-273 (1996b).

Kolmogorov, A. N. Akad. Nauk SSSR 32, 19 (1941).

Krishnamurti, R. "Low Frequency Oscillations in Turbulent Rayleigh-Bénard Convection" preprint (1995).

Malkus, W. V. R. "Outline of a theory of turbulent convection." In Theory and Fundamental Research in Heat Transfer, (ed. J. A. Clark). Pergamon Press, Tarrytown (1963).

Maxworthy, T. & Narimousa, S. "Unsteady deep convection in a homogeneous rotating fluid." J. Phys. Oceanogr. 24, 865–887 (1994).

McWilliams, J. C. "The boundary layer dynamics of symmetric vortices." Ph.D. thesis, Harvard University, unpublished (1971).

Melander, M. V., Zabusky, N. J. & McWilliams, J. C. "Symmetric vortex merger in two dimensions: causes and conditions." J. Fluid Mech. 195, 303–340 (1988).

Moeng, C.-H. & Rotunno, R. "Vertical Velocity Skewness in the Buoyancy-Driven Boundary Layer." J. Atmos. Science 47, 1149-1162 (1990).

Nakagawa Y. & Frenzen, P. "A theoretical and experimental study of cellular convection in rotating fluids." Tellus 7, 1–21 (1955).

Prandtl, L. "Meteorologische Anwendungen der Strömungslehre." Beitr. Physik fr. Atmos. 19, 188–202 (1932).

Priestley, C. H. B. "Convection from a large horizontal surface." Austral. J. Phys. 7, 176–201 (1954).

Priestley, C. H. B. "Turbulent transfer in the lower atmosphere." The University of Chicago Press. Chicago & London (1959).

Sano, M., Wu, X.-Z. & Libchaber, A. "Turbulence in helium-gas free-convection." Phys. Rev. A 40, 6421–6430 (1989).

She, Z.-S. "On the scaling laws of thermal turbulent convection." Phys. Fluids A 1, 911–913 (1989).

Shen, Y., Xia, K.-Q. & Tong, P. "Measured Velocity Boundary Layers in Turbulent Convection" Phys. Rev. Lett. 75, 437 (1995).

Shen, Y., Xia, K.-Q. & Tong, P. "Turbulent Convection over Rough Surfaces" Phys. Rev. Lett. 76, 908–911 (1996).

Shraiman, B. & Siggia, E. "Heat transport in high-Rayleigh-number convection." Phys. Rev. A 42, 3650–3653 (1990).

Spiegel, E. A. "On the Malkus theory of turbulence." Mécanique de la turbulence, Colloque Internationaux de CNRS a Marseille, pp. 181-201. Éditions CNRS (1962).

Tennekes, H. & Lumley, J. L. "A First Course in Turbulence" MIT, Cambridge, MA (1972).

Werne, J. "The structure of hard-turbulent convection in two dimensions: numerical evidence." Phys. Rev. E 48, 1020–1035 (1993).

Werne, J. "2D Convection in Tall Narrow Containers: Implications for Theories of Heat Transport in Hard Turbulence." in preparation (1996).

Wu, X.-Z. & Libchaber, A. "Scaling relations in thermal turbulence—the aspect-ratio dependence." Phys. Rev. A 45, 842–845 (1992).

Yakhot, V. "4/5 Kolmogorov law for statistically stationary turbulence: application to high-Rayleigh-number Bénard convection." Phys. Rev. Lett. 69, 769–771 (1992).

Zhong, F., Ecke, R. & Steinberg, V. "Rotating-Bénard convection: asymmetric modes and vortex states." J. Fluid Mech. 249, 135–159 (1993).